Queensland University of Technology
Brisbane Australia

This may be the author's version of a work that was submitted/accepted for publication in the following source:

Rathnayaka Mudiyanselage, Charith Malinga, Karunasena, H.C.P., Senadeera, Wijitha, & Gu, YuanTong
(2018)
Application of 3D imaging and analysis techniques for the study of food plant cellular deformations during drying.
Drying Technology, *36*(5), pp. 509-522.

This file was downloaded from: https://eprints.qut.edu.au/223063/

© Consult author(s) regarding copyright matters

This work is covered by copyright. Unless the document is being made available under a Creative Commons Licence, you must assume that re-use is limited to personal use and that permission from the copyright owner must be obtained for all other uses. If the document is available under a Creative Commons License (or other specified license) then refer to the Licence for details of permitted re-use. It is a condition of access that users recognise and abide by the legal requirements associated with these rights. If you believe that this work infringes copyright please provide details by email to qut.copyright@qut.edu.au

Notice: *Please note that this document may not be the Version of Record (i.e. published version) of the work. Author manuscript versions (as Submitted for peer review or as Accepted for publication after peer review) can be identified by an absence of publisher branding and/or typeset appearance. If there is any doubt, please refer to the published source.*

https://doi.org/10.1080/07373937.2017.1341417

Application of 3-D Imaging and Analysis Techniques for the Study of Food Plant Cellular Deformations during Drying

Journal:	*Drying Technology*
Manuscript ID	LDRT-2017-0120.R2
Manuscript Type:	General Paper
Date Submitted by the Author:	n/a
Complete List of Authors:	Rathnayaka, Charith; Queensland University of Technology Faculty of Science and Engineering, School of Chemistry, Physics and Mechanical Engineering; University of Moratuwa, Department of Chemical and Process Engineering Karunasena, H. C. P.; University of Ruhuna Faculty of Engineering, Department of Mechanical and Manufacturing Engineering senadeera, wijitha; Queensland University of Technology Faculty of Science and Engineering, School of Chemistry, Physics and Mechanical Engineering; University of Southern Queensland - Springfield Campus, Department of Mechanical and Electrical Engineering Gu, Yuan; Queensland University of Technology Faculty of Science and Engineering, School of Chemistry, Physics and Mechanical Engineering
Keywords:	Food drying, Plant tissues and cells, 3-D imaging, 3-D modelling and simulation, Morphological variations, Experimental findings

For Peer Review

SCHOLARONE™
Manuscripts

Application of 3-D Imaging and Analysis Techniques for the Study of Food Plant Cellular Deformations during Drying

C. M. Rathnayaka [1, 2], H. C. P. Karunasena[3], W. Senadeera[1,4,] and Y. T. Gu[1] *

[1] Queensland University of Technology (QUT), Science and Engineering Faculty, School of Chemistry Physics and Mechanical Engineering, Brisbane, Australia

[2] Department of Chemical and Process Engineering, Faculty of Engineering, University of Moratuwa, Moratuwa, Sri Lanka

[3] Department of Mechanical and Manufacturing Engineering, Faculty of Engineering, University of Ruhuna, Hapugala, Galle, Sri Lanka

[4] Department of Mechanical and Electrical Engineering, University of Southern Queensland, Springfield, Queensland, Australia

[*] Corresponding author: School of Chemistry Physics and Mechanical Engineering, Science and Engineering Faculty, Queensland University of Technology, 2 George Street, Brisbane QLD, 4001 Australia.

Tel: +61-7-3138 1009; Fax: +61-7-3138 1469; E-mail: yuantong.gu@qut.edu.au

For Peer Review Only

ABSTRACT

In this investigation, novel 3-D imaging and image-analysis tools have been employed to observe the deformations of food-plant tissues and single cells during convective air drying at 70 °C. A comprehensive investigation was carried out to qualitatively and quantitatively analyse the shrinkage and surface wrinkling of Royal Gala apple parenchyma cellular structure during drying. To study the cellular morphology, 3-D contour maps produced by a novel 3-D image and surface analysis tool, 'Nanovea Expert 3-D' were employed. ImageJ software was used to quantify the single cell morphological characteristics. During the study, each tissue was observed continuously for the gradual morphological alterations. It was evident that there is a significant reduction of surface roughness during the drying process. In the case of individual cells, the area reduced approximately by 20% and diameter by 11%. This study provides conclusive proof that 3-D contour maps and images combined with the 2-D microscopic images could be a highly valuable source of information in producing data for the validation of 3-D computational plant tissue drying models and simulations.

Keywords: Food drying; Plant tissues; 3-D imaging; 3-D modelling and simulation; Morphological variations; Experimental findings

1. INTRODUCTION

Drying is one of the most common and cost effective techniques for preservation of food and for the production of traditional as well as innovatively processed products [1]. It is employed to increase the shelf life of approximately 20% of the planet's perishable crops [2]. During drying, the moisture levels of food matter are brought down in order to increase the shelf life by decelerating numerous biological activities. With the removal of water, cellular structures of the food materials undergo structural deformations that have serious impacts on drying operational performance, dried food quality and their eventual market value [3-6]. In order to engineer feasible food drying operations, it is important that these cellular structural deformations are optimally controlled. In that context, a thorough understanding on underlying solid and fluid dynamics is critical. However, because of the very small size and heterogeneity of the plant cells and tissues, it is difficult to observe and distinguish the morphological phenomena present in the plant cellular structure with the naked eye [7]. In order to overcome this, researchers use numerous tools and techniques. Microscopy is one such technique where images of the real plant cellular structure are magnified in order to help researchers to identify the true mechanisms taking place in the cellular structure. There are various microscopy techniques categorised according to the method of image enlargement and distinguishing: optical microscopy, scanning probe microscopy and electron microscopy. There are numerous sub categories under these main categories and lots of studies have been implemented employing such techniques [8, 9] on plant cells and tissues.

Through further experimentation, it has been found that the key factors influencing the morphological characteristics in food plant cellular structure during drying are the moisture

For Peer Review Only

content [10-15] and the drying temperature [16]. To derive the most appropriate relationship among these influencing factors, research has been conducted in areas such as: cellular morphogenesis and underlying transport phenomena [17-20], leading to various microscale theoretical [21, 22] and empirical [10, 12, 23] models. Recently, numerical modelling has attracted increased attention as a viable tool for the advanced analysis of micro-structural morphological behaviour [24-30]. It is believed that such improved numerical models can immensely benefit food engineering in terms of optimising drying process performance and product quality [31-33]. However, it is critical to validate these numerical models before using for the prediction of the unknown. In doing so, the experimental findings on true plant cellular structure are necessary. For this purpose, various types of microscopic imaging and other techniques have been used according to the literature. As sophisticated numerical models are being developed, validation of such models are also becomes further challenging. Accordingly, the numerical models developed for plant tissue drying are mainly limited to two-dimensions (2-D) [26, 30, 34-36], requiring just 2-D microscopic experimental data to be used for the validation such as the ones obtained from scanning electron microscopy (SEM) [10, 37]. However recently, 3-D cellular drying models have been being developed [38]. This has created the necessity of 3-D microstructural experimental data for the validation of such models [37]. In this background, we aim to produce microscopic information which could be used to validate the predictions of a 3-D numerical modelling and simulation study on drying phenomena in the food-plant cellular structures. By doing so we intend to fill that gap through visualisations and quantifications of the 3-D microstructural morphological changes in food-plant tissues during drying with the aid of powerful and novel microscopic imaging and analysis techniques.

2. MATERIALS AND METHODS

2.1. Materials and Sample Preparation

For Peer Review Only

For the experiments, Royal Gala apple (*Malus Domestica*) procured from Brisbane (Australia) were used, which were stored at 4 °C in a refrigerator for three days before using for the sample preparation. During sample preparation, the apples were washed with clean water and slices having dimensions of 1 cm × 1 cm × 2 mm (thickness) were then cut from the middle parenchyma region using a sharp knife. In order to assist microscopic imaging, all the fresh samples were stained with a Toluidine Blue 1% in Sodium tetraborate solution (TB). TB is a dye with high affinity commonly used for enhancing the appearance of plant and animal tissues under the optical microscopy and TB does not cause any additional dehydration [39, 40].

For drying, a convective air dryer (Excalibur's five-tray dehydrator, USA) was used which has an electric heater and a fan to produce a controlled hot air flow across the samples throughout the experiments. The air temperature can be conveniently adjusted using a thermostat. For this particular series of experiments, an air temperature of 70 °C with a constant hot air velocity was maintained. The samples were kept symmetrically on the same tray in close proximity to the central axis and air inlet vent of the equipment to ensure a uniform heat transfer throughout. The samples were introduced only after the dryer reaches the steady state condition following the initial warming-up cycle. The apple samples were placed only in the middle three trays out of the five available trays while other remaining trays were removed from the dryer. It should be noted here that in order to capture the gradual morphological changes of the samples in each drying experiment, the same apple sample was used and intermittently observed using the microscope. A given apple sample was dried for 3 minutes and was taken out of the dryer for the observation under the microscope and eventually the samples were weighed and placed back in the dryer for further drying for 3 minutes for the next measurement cycle and so on. Once the samples were taken out from the dehydrator, it was kept in a small-sized desiccator in order to avoid partial

For Peer Review Only

rehydration due to the lab ambient conditions. No desiccant was used to make sure that no further dehydration occurred during this time period between the samplings. This procedure was repeated until the weight of the sample became constant in two adjacent measurements, implying a fully dried state. Sections below describe the use of different microscopic techniques for the observation of the samples and the corresponding results obtained.

2.2. Observations through the Digital Light Microscopy

The microstructure of the TB stained fresh samples were observed under the Leica DM6000M digital light microscope before and throughout the dehydration process. Staining of the sample with TB enhances the clarity of the microscopic image through making cell wall membranes more distinct. It has no impact on z-directional stacking or corresponding 3-D effects created during image analysis due to the one-time staining. There was no further requirement to stain the image during or after dehydration. This microscope could be used for observations under both the incident and transmitted light with an automated contrast and light management. In each case, images were taken at a resolution of 1352 × 1000 pixels using Z-stacked acquisition for better focus and clarity. z-stacking (or focus stacking) is a digital image processing technique where multiple images taken at different focal lengths are combined together to eventually generate a composite image with a greater depth of field [41, 42]. Due to the Z direction stacking of the images, the 3-D aspect of the obtained images were enhanced and it was helpful in making a better analysis on the experimental findings. The process of generating an image with 3-D effects has been visually represented in Fig. 1. It outlines how the images taken at different focal lengths are combined through focus stacking (or z-stacking) to generate the final image with 3-D effects. The real number of images taken at different focal lengths are usually larger than 30. However, in Fig. 1, only a few have been shown for the sake of simplicity.

For Peer Review Only

The imaging was done at three different magnifications: 5 (5M), 10 (10M) and 20 (20M) facilitating the analysis procedure. The values 5, 10 and 20 in 5M, 10M and 20M magnifications are respectively the magnification of the first lens kit of the microscope. While further processing the image through the microscope itself as well as the computer program which eventually gives the output, the magnification of the image becomes much higher. In Fig. 2, the experimental procedure has been mapped out. When moving on to a higher magnification, only a smaller section of the existing image was zoomed in and refined with focussing techniques. The number of cells present inside the image decreased with increasing magnification.

2.3. Moisture Content Measurements and Analysis

In order to determine the moisture content of the samples, it was not possible to employ the standard AOAC method 934.06 (1995) which has been utilised in a number of previous similar studies due to the absence of a vacuum pump to attain the necessary degree of vacuum [37]. Alternatively, a weight-based method was employed, where the weight of the fresh samples were measured before and after the drying process using a digital weighing scale (KERN & Sohn GmbH, ABJ 220-4M, Germany). As it has been mentioned previously, one of the key highlights of this work is to experimentally observe the gradual changes of the morphology of the plant cells and tissues during drying. Therefore, the obtained microscopic images corresponding to different states of drying were analysed using the normalised moisture content of each sample (X/X_0) obtained by dividing the moisture content (X) of a sample at each measurement instance by the moisture content corresponding to the fresh state (X_0) of the sample. It should be noted here that the experiments and all the corresponding measurements (not only moisture content) were repeated three times. The average value of the three measurement iterations were taken as the representative value of the analysis. All the graphical representations in this article have been developed based on these values.

For Peer Review Only

2.4. Analysis of the Images

One of the key highlights of this study is that the same sample has been used for every measurement. The same location or the site in a given tissue sample is observed and imaged using the microscope. The focus was placed on the overall morphological behaviour of the cellular structure first. After examining the whole sample through the microscope, a site which would represent the whole sample's general morphological characteristics was identified. Consequently, this study becomes more accomplished compared to a number of previous similar studies which have used separate samples to investigate different states of dryness [37]. For the quantitative analysis of the experimental images, the image processing software, ImageJ was employed [43, 44]. The selected cells of the imaged sample were measured for area and perimeter. Using these data, the degree of shrinkage of the cells were determined and the comparability of the results were improved by normalising each parameter.

2.5. Software based 3-D Tissue Model Generation and Analysis

To further strengthen the analysis, the digital light microscopic images of the plant cellular structure were then investigated through a special 3-D software tool 'Nanovea Expert 3D' (Version 6.2.6409). This software is a specialist surface examination and profiling tool. It is a customised version of Digital Surf's Mountains® software [45-47]. It could be used for both 2-D and 3-D analytical work, especially for surface analysis. For this process, a series of z-stacked microscopic images are needed. These were obtained through the experimental procedure explained in the Section 2.2. For each drying state, the corresponding z-stacked images were used by this particular software in order to re-create the 3-D surface morphology of the tissue as seen from the z-direction, using a 3-D contour map. This was implemented through re-establishing the final montage image from the z-stacked images in the Nanovea Expert 3-D environment as a studiable project. In this 3-D contour map, the depth of the

For Peer Review Only

image was well elaborated. Consequently, the qualitative and quantitative 3-D analysis of the cells and the tissues became much more convenient, compared to the pure microscopic images, which are essentially 2-D. For instance, 3-D contour maps can quantify the surface roughness, maximum height and root mean square height of the contours in the real tissue, which is almost impossible to quantify just using the conventional 2-D image analysis techniques [45, 48]. The next section present further details of the 3-D image analysis conducted and the results obtained.

3. RESULTS AND DISCUSSION

3.1. Drying Kinetics

The overall trend of moisture content reduction during the drying cycle of a tissue sample, the drying curve is presented in Fig. 3, which was drawn based on the normalised moisture content values. The corresponding experimental data and statistical analysis is presented in Table 1. It is noteworthy that identifying a constant rate drying period is difficult as reported in similar previous studies [37, 49]. It should be mainly due to the small thickness of the tissue used for the experiment and the relatively higher temperature of drying (70 ^{0}C). Due to these, the sample gets rapidly dried by effective removal of moisture from external boundaries and internal regions. However, the falling rate drying period is clearly visible from time 0 min to 32 min and eventually the sample reached the steady fully dried state from time 32 min to 42 min.

3.2. Analysing the Degree of Shrinkage and other Morphological Characteristics through Digital Light Microscopy

The digital light microscopy images obtained at tissue scale for the same apple sample during drying is shown in Fig. 4 where, the shrinkage and surface wrinkling phenomena occurring during drying are evident. The wrinkling behaviour of the surface is much more evident through the 20M microscopic images compared to the 5M microscopic images. At t =

For Peer Review Only

0 min, the fresh cellular structure is shown. Compared to the microscopic images of the same sample at dried state (e.g. at t = 42 min), the fresh cellular structure exhibits an inflated spherical nature due to the higher cell turgor pressure and the corresponding higher stresses of the cell wall membrane [7, 15, 37, 50-53]. Thereafter, a higher degree of shrinkage could be observed in the dried cellular structure along with surface wrinkling as presented in the images (when $t > 0$ min). It is noteworthy that the State-of-the-art numerical studies on food-plant cellular deformations during drying have mainly outlined morphological description in terms of shrinkage. Therefore in this study, we mainly focused on quantitatively assessing shrinkage phenomena instead of surface wrinkling as our main aim was to produce experimental findings which could validate such numerical modelling work.

The key driving forces behind these variations are moisture gradient and the associated turgor pressure difference. The recently reported Scanning Electron Microscopy (SEM) based experimental studies on the drying of the apple cellular structure explains such microstructural changes as a two-staged process [54]. Further, the voidage or porosity in the plant cellular structure increases with the dryness as observed from the images corresponding to $t \geq 36$ min. This phenomenon is further evident when inspecting a wider area of the tissue image covering a higher number of the cells under lower magnification (i.e. the 5M and 10M magnifications). These cause increments in the bulk porosity and decrements in the bulk density.

There is a crucial involvement of the intercellular spaces for the microstructural morphological behaviour of the plant cellular structure. The fresh cellular structure demonstrates a more tightly packed behaviour (t = 0 min in Fig. 4), compared to the extremely dried state of the same sample (t = 42 min in Fig. 4), where the cells become relatively loosely packed. This is in alignment with the previous research using SEM images

For Peer Review Only

of the cellular structure of apple revealing the existence of expansions and newly formed intercellular spaces during drying [54]. The trend is mainly caused by the escape of the entrapped moisture and expansion of trapped air and vapours in the intercellular compartments.

It could be observed that there is a considerable difference in the colour of the images where the fresher tissues appear in purple colour while dried tissues appear in dark blue colour. This was not caused by the properties of the cellular structure. This can be attributed to the discolouration of the used staining agent (i.e. Toluidine Blue solution) with drying [39]. This discolouration was validated by simultaneously looking at the dehydrated apple cellular structure images which were not stained.

3.3. 3-D Contour Maps Obtained through Expert 3-D for Tissue Images

In Fig. 5(a) the microscopic image corresponding to fresh apple tissue under 20M is shown and in Fig. 5(b), the 3-D contour map for the same tissue section produced through the Nanovea Expert 3D software is given. In Fig. 5(c), the 3-D isometric view of the same 3-D contour map is shown. The arrows in the Fig. 5(a) and (b) denotes the comparability between the visualisations. It is evident that the 3-D contour map gives out more details about the depth of the sample, which cannot be directly obtained from the original 2-D microscopic image. The 3-D contour map reveals more 3-D information about the cellular surface such as surface roughness (S_a), maximum height (S_z) and root mean square height (S_q) of contours. The digital light microscopic images reveal information only on the X and Y planes while the Expert 3-D image generates information with respective to all the X, Y and Z planes. Particularly the Z axis depth variation of the plant cellular structure during drying is a critical factor in analysing the real morphological variations of the food-plant cellular structure. These 3-D images combined with the 2-D microscopic images could be a highly valuable

For Peer Review Only

source of information in producing information for the validation of 3-D numerical plant tissue drying models and simulations [38].

In determining the quantitative details about a particular surface, this analytical tool employs the ISO 25178 standard relating to the analysis of 3-D areal surface texture. In Fig. 6, a data set produced for a fresh apple sample is shown, where the Fig. 6(a) presents the 2-D view corresponding to the 3-D contour map indicated in Fig. 5. The Fig. 6(b) displays quantified surface information corresponding to the sample. In order to study the variation of the 3-D characteristics of the plant cellular structure during drying, the Expert 3-D data obtained for the same apple sample at various states of dryness were analysed. The results are presented in Table 1 along with the corresponding statistical analysis. S_a, S_z and S_q were chosen as the key parameters that could be used to demonstrate the 3-D behaviour (see Fig. 7)

An overall reduction of surface roughness (S_a), maximum height (S_z) and the root mean square height (S_q) could be generally observed from Fig. 7. There is a rapid reduction of the sample height with the increasing degree of dryness in the initial stages ($1.0 \geq X/X_0 \geq 0.5$) (Fig. 7(a).) Thereafter, it becomes negligible, revealing that the surface roughness reduces initially at a higher rate and then remains unchanged during the latter part of the operation. A similar trend is observed with respective to the maximum height (S_z) and the RMS height (S_q), as observed from Fig. 7(b) and (c). It provides conclusive evidence that not only the x, y planes but also the z direction gets involved in the morphological variations eventually leading to overall reductions of volume (i.e. cellular structural shrinkage) [10, 37].

3.4 Single Cell Observations and Quantification of Morphological Changes

For single cell observations, a separately prepared apple sample was used than the one that was used for tissue experiments. However, procedures were followed similar to that of

For Peer Review Only

tissue experiments regarding sample preparation and dehydration. At the same time, the moisture content measurements were also done corresponding to each dryness level. Using the 50M magnification (true magnification approximately 1000) of the Leica DM6000M digital light microscope, a single cell was observed in the apple cellular structure. This was carried out as a series of observations targeting a selected single cell of a given sample in order to capture the gradual morphological changes of it, as drying progresses. The resulting microscopic images are shown in Fig. 8. These images provide vital information on the 3-D surface morphological changes present in the single cell scale of the food-plant microstructure. For instance, the surface wrinkling behaviour of the cell wall during the drying process is clearly visible in this series of images. Initially, the wrinkled nature of the cell wall surface is hardly visible (see Fig. 8(a)-(b)). As the drying progresses, the wrinkles start to form on the surface (see Fig. 8(c)-(e)). In the extreme dryness states, the cellular surface demonstrates a highly wrinkled behaviour (see Fig. 8(j)-(l)). The overall shrinkage of the cell exhibits a similar trend to that of the surface wrinkling throughout the drying process. Due to the 3-D nature of these images, the micro-level surface details become further evident. To further emphasize the difference between the fresh and dried conditions, Fig. 9 shows two enlarged images. Fig. 9(a) presents and enlarged microscopic image of the fresh cell and Fig. 9(b) presents its extremely dried condition.

Using these high-resolution images, the morphological behaviour of the observed cell during drying was quantified via the image processing techniques found in the ImageJ software. As it could be seen in Fig. 8, the cell was easily distinguishable in all dryness states. Therefore, any image segmentation was not necessary during image processing. For this analysis, mainly the area, perimeter along the major and minor axes of the cell were quantified for each image as the basic measurements. Next, geometric parameters such as Feret diameter and roundness were derived to strengthen the analysis using those basic

For Peer Review Only

measurements. The Feret diameter [1] was measured in this investigation through the area of the cell. It should be noted here that obtaining z-stacked images at this very high level of magnification was a difficulty. This issue became further severe for dried samples. As a consequence, apart from the Fig. 8(a) and (b), any of the single cell images presented in Fig. 8 were not z-stacked. Further details on this technical issue will be discussed in Section 3.5.

In order to quantify and compare the cellular morphological characteristics, a number of cellular geometrical parameters were used in alignment with the recently reported analogical studies [37]. They are: cell area (A), Feret diameter (D) and roundness[2] (R). The variation of these parameters were analysed with the dry basis moisture content X ($mass_{water}/mass_{dry\ solid}$). For better comparison and analysis, these parameters were normalised (X/X_0, A/A_0, D/D_0 and R/R_0) by dividing the steady state value of a given parameter by its initial value corresponding to the fresh cell state (X_0, A_0, D_0 and R_0). These quantified morphological properties were then compared against the experimental findings available in literature [10, 34, 54]. The quantified morphological characteristics along with the time and moisture content variations are given in Table 2. In addition, the corresponding standard deviations have also been included. Next, the variations are graphically shown in the plots given in Fig. 10– Fig. 12.

The 2-D surface area of the single cell used in this analysis ranged from around 12100 μm^2 to around 9800 μm^2 leading to approximately 20% reduction during the drying process. From the area variation during drying, it could be seen that the cells experience a significant area shrinkage while going through the process. In the fresh apple samples, the Feret diameter varied from approximately 125 μm to approximately 112 μm (approximately 11% reduction)

[1] $\sqrt{4A/\pi}$
[2] $4\pi A/P^2$

For Peer Review Only

during drying. It can be observed that compared to the area variation, the diameter variation is considerably smaller. The roundness of the fresh apple cells was in the range of 0.80. This figure leads to an implication that the fresh apple cells are not quite circular (or spherical). Throughout the drying process, the roundness of the cell stayed around the same value of 0.80. Even though the roundness of cells is expected to drop after drying, through these experiments it was observed that the roundness stays almost constant regardless of the increasing degree of morphological changes in the entire tissue. One of the reasons behind this phenomenon is the generation and evolution of round-shaped intercellular spaces during the operation [37]. Such spaces (or voids) usually possess comparable sizes to those of the apple cells in the systems as seen in Fig. 4.

As we have measured the same single cell during the entire experimental procedure, the results derived through our studies could be considered more reliable than most of the investigations reported in literature which have used different tissue samples for different dryness states. According to the cell area variation graphs presented in Fig. 10, when the normalised moisture content varies from 1.0 to 0.0, the normalised cell area varies from 1.0 to approximately 0.8 during the time interval of the drying operation. In other words, during the drying operation, the area of the cell reduces approximately 20 %. This implies that there is a significant variation in the cell morphological characteristics during drying. The cell Feret diameter variation during drying is graphically presented in Fig. 11. As seen from the graphs, the Feret diameter shows a decreasing trend throughout the operation. The normalised diameter varies from 1.0 to approximately 0.9 while moving from a fresh state to an extremely dried state. Hence, there is an approximately 10% reduction of Feret diameter occurring as a consequence of drying.

For Peer Review Only

When further analysing Fig. 10 and Fig. 11, it could be observed that there are drastic changes in the morphological characteristic variations at extremely dried states (i.e. $X/X_0 \leq 0.25$). Previous researchers have used a theory of glass transition in order to explain such kind of extreme shrinkage and associated phenomena demonstrated by food cellular structures during drying [37, 55, 56]. Such work state that these significant changes of morphological behaviour could occur only if the drying process temperature is above a particular glass transition temperature which is specific to the material in a given moisture content.

At the same time, the theories of case hardening seems to be appropriate for explaining these characteristic trends [57-60]. Case hardening occurs where the outer cell layers tend to undergo higher rates of drying and shrinkage leading to an excessively hardened case which partially prohibits moisture transport from interior tissue regions to the exterior [26]. Consequently, the shrinkage of the inner parts of the material decelerates. Case hardening is more dominant in relatively higher temperatures. If a lower temperature is occupied, the initial rate of moisture transfer from the material would be slower but there would be a relatively more uniform moisture transport when the entire sample is considered. This would result in a higher total shrinkage when the entire process is considered. This phenomenon has been experimentally observed for apple under convective air drying [58, 61].

The variation of the normalised cell roundness is shown graphically in Fig. 12. It could be observed that the normalised cell roundness stays close to 1.0 throughout the entire drying operation. This suggests that the roundness of the dried cell has not varied considerably compared to the fresh state roundness. It could be a dynamic process as discussed above and shown in Fig. 12. In addition, in the 3-D images shown in Fig. 8 and Fig. 9, it could be observed that 2-D and 3-D analyses on cell roundness agree with each other. One probable

For Peer Review Only

cause behind this is the contribution of the outer shape of the cell towards estimation of the roundness. Nevertheless, it is noteworthy that in the 3-D analysis, when z-directional details of the cell wall surface are considered, new valuable information could be obtained compared to an analysis which is constrained to 2-D. However, when the eventual outcome is considered, it could be stated that the degree of roundness does not change significantly during the process. The geometric parameter variations of the Royal Gala apple cells observed in this study seem to be comparable with the Idared and Golden Delicious apple cells reported in a number of previous studies [15, 37].

3.5. 3-D Contour Maps for Single Cells

The 3-D contour map obtained for a fresh single cell through Expert 3-D surface analysing software is shown in Fig. 13. For the sake of easy comparison, Fig. 13(a) shows the digital light microscopic image for the fresh apple sample taken at 50M while in Fig. 13(b), the corresponding 3-D contour map is shown. The arrow and the circulated areas denote the analogical sites of the microscopic image and the 3-D contour map. This analogy between Fig. 13(a) and Fig. 13(b) is a good indication of the validity of the 3-D contour maps and consequently the surface morphological data produced. This is one of the key highlights derived through this study. The application of 3-D surface profiling tools in the context of a single cell microscopic observation is a novel technique. It can be used to produce microscopic morphological information to validate 3-D numerical modelling and simulation studies on drying phenomena in the food-plant cellular structures. In literature, experimental studies that provide such useful validation information are extremely rare. Therefore, this information obtained through single cell microscopic observation and 3-D surface analysing tools could be considered vital in this area of study.

The corresponding 3-D surface texture analysis is presented in Fig. 14. Surface profile of the fresh apple sample is shown in Fig. 14(a), while the surface parameters including the

For Peer Review Only

surface roughness (S_a) is given in Fig. 14(b). This information can be helpful for a comprehensive comparison with surface morphological characteristic predictions of a modelling and simulation study on a fresh single plant cell. However, when it comes to the observation of plant cellular structure at this level of magnification, obtaining of z-stacked images was a difficulty due to the limitations exist in the instrumentation used in this experimental investigation. At this relatively 'very high' magnification (50M), the microscope should possess the ability to change its focal length in very fine distance intervals in order to obtain a clear z-stacked image. The instrument used in this study had some difficulties in this area. And Expert 3D software needs z-stacked images for the creation of 3-D contour maps. Moreover, since they were not taken as z-stacked images, the 3-D contour maps of the dried single cell images could not be obtained. Nevertheless, single cells could be imaged clearly without the support of z-stacking (Fig. 8 and Fig. 9 above).

4. CONCLUSION

A comprehensive Digital Light Microscopy-based investigation was carried out on Royal Gala apple parenchyma cells. This investigation intended to produce experimental findings that could be used to validate 3-D numerical modelling studies on plant cellular structure during drying. One of the key highlights of this study was the ability to closely observe a single cell and then study its morphological behaviour. The fresh cellular structure demonstrates an inflated nature due to the equilibrium between the turgor pressure and the stresses of the cell wall membrane. During drying, cells demonstrate a significant degree of shrinkage and surface wrinkling due to the moisture removal and associated turgor loss. 3-D contour maps obtained through 'Nanovea Expert 3-D' reveal information regarding the depth (or z-axis dimensions) of the sample which cannot be directly extracted by looking at 2-D microscopic images.

For Peer Review Only

Findings of this investigation show that the surface roughness (S_a) of apple tissues declined gradually during the drying process approximately 20%. Both maximum height (S_z) and root mean square height (S_q) dropped approximately 20% and 16%, respectively. The area of a single cell demonstrated approximately a 20% reduction during drying. The Feret diameter reduced approximately 11% while the roundness stayed around the same value of 0.80 throughout. These parameter variations show that there is a drastic change in the single cell morphological behaviour at extremely dried states. This phenomenon has been explained with theories related to glass transition temperature and case hardening. If a numerical model is going to be developed to simulate the morphological behaviour of food plant cellular structure during drying, it should allow approximation of large deformations as well as significant shrinkage and surface wrinkling. The selected method should be able to cope with extreme moisture content variations and associated changes of morphological characteristics.

The analytical and experimental methodologies discussed in this investigation could be used for analysing the plant cellular structure in further detail. To further study the surface wrinkling behaviour of plant cellular structure in a quantitative manner, ImageJ software could be used. Such studies will be helpful in deriving experimental information that can be used to better understand the mechanisms that are taking place in the plant cellular structure during drying. In addition, such information could be used together with numerical modelling studies in order to improve food drying operations in terms of product quality, nutritional content and eventual market value.

ACKNOWLEDGEMENTS

Firstly, the support from the ARC Discovery Project (DP150100828) and ARC Linkage Project (LP150100737) should be acknowledged here. The authors of this study kindly acknowledge: the support given by the experimental facilities and expertise (especially

For Peer Review Only

Dr. Sanjleena Singh) provided by Central Analytical Research Facility (CARF) of Queensland University of Technology (QUT), Brisbane, Queensland, Australia; the financial support provided by the Chemistry, Physics and Mechanical Engineering (CPME) scholarship provided by the Science and Engineering Faculty (SEF), QUT. The first author specifically extends the sincere support provided by University of Moratuwa, Sri Lanka.

REFERENCES

1. Jangam, S.V. An overview of recent developments and some R&D challenges related to drying of foods. Drying Technology 2011, 29 (12), 1343-1357.

2. Stefan, G.; Hosahalli, S.R.; Michele, M.; Drying of fruits, vegetables, and spices. In Handbook of Postharvest Technology: Cereals, Fruits, Vegetables, Tea, and Spices; CRC Press: 2003; 653-695.

3. Wong, E.H. Characterizing the kinetics of free and bound water using a non-isothermal sorption technique. Drying Technology 2017, 35 (1), 46-54.

4. Kermani, A.M.; Khashehchi, M.; Kouravand, S.; Sadeghi, A. Effects of intermittent microwave drying on quality characteristics of pistachio nuts. Drying Technology 2016, 1-9.

5. Vu, H.T.; Scarlett, C.J.; Vuong, Q.V. Effects of drying conditions on physicochemical and antioxidant properties of banana (musa cavendish) peels. Drying Technology 2016, 1-11.

6. Würth, R.; Foerst, P.; Kulozik, U. Effects of skim milk concentrate dry matter and spray drying air temperature on formation of capsules with varying particle size and the survival of microbial cultures in a microcapsule matrix. Drying Technology 2017.

7. Taiz, L.; Zeiger, E. Plant Physiology; Sinauer Associates: New York, 2002.

8. Aguilera, J.M.; Stanley, D.W. Microstructural Principles of Food Processing and Engineering; Springer Science & Business Media: 1999.

9. Aguilera, J.M.; Chiralt, A.; Fito, P. Food dehydration and product structure. Trends in Food Science & Technology 2003, 14 (10), 432-437.

10. Mayor, L.; Silva, M.; Sereno, A. Microstructural changes during drying of apple slices. Drying Technology 2005, 23 (9-11), 2261-2276.

11. Lozano, J.E.; Rotstein, E.; Urbicain, M.J. Total porosity and open-pore porosity in the drying of fruits. Journal of Food Science 1980, 45 (5), 1403-1407.

12. Ramos, I.N.; Silva, C.L.M.; Sereno, A.M.; Aguilera, J.M. Quantification of microstructural changes during first stage air drying of grape tissue. Journal of Food Engineering 2004, 62 (2), 159-164.

13. Hills, B.P.; Remigereau, B. NMR studies of changes in subcellular water compartmentation in parenchyma apple tissue during drying and freezing. International Journal of Food Science & Technology 1997, 32 (1), 51-61.

14. Lee, C.Y.; Salunkhe, D.K.; Nury, F.S. Some chemical and histological changes in dehydrated apple. Journal of the Science of Food and Agriculture 1967, 18 (3), 89-93.

For Peer Review Only

15. Lewicki, P.P.; Pawlak, G. Effect of drying on microstructure of plant tissue. Drying Technology 2003, 21 (4), 657-683.

16. Ratti, C. Hot air and freeze-drying of high-value foods: A review. Journal of Food Engineering 2001, 49 (4), 311-319.

17. Bolin, H.; Huxsoll, C. Scanning electron microscope/image analyzer determination of dimensional postharvest changes in fruit cells. Journal of Food Science 1987, 52 (6), 1649-1650.

18. Chaplain, M.A. The strain energy function of an ideal plant cell wall. Journal of Theoretical Biology 1993, 163 (1), 77-97.

19. Hettiaratchi, D.; O'Callaghan, J. Structural mechanics of plant cells. Journal of Theoretical Biology 1978, 74 (2), 235-257.

20. Lewicki, P.; Drzewucka-Bujak, J. Effect of drying on tissue structure of selected fruits and vegetables. In Proceedings of the 11th International Drying Symposium, Halkidiki, Greece, August 19-22, 1998; 1093-1099.

21. Crapiste, G.H.; Whitaker, S.; Rotstein, E. Drying of cellular material—I. A mass transfer theory. Chemical Engineering Science 1988, 43 (11), 2919-2928.

22. Zogzas, N.; Maroulis, Z.; Marinos-Kouris, D. Densities, shrinkage and porosity of some vegetables during air drying. Drying Technology 1994, 12 (7), 1653-1666.

23. Karathanos, V.; Villalobos, G.; Saravacos, G. Comparison of two methods of estimation of the effective moisture diffusivity from drying data. Journal of Food Science 1990, 55 (1), 218-223.

24. Karunasena, H.C.P.; Senadeera, W.; Gu, Y.T.; Brown, R.J. A coupled SPH-DEM model for micro-scale structural deformations of plant cells during drying. Applied Mathematical Modelling 2014, 38 (15–16), 3781-3801.

25. Karunasena, H.C.P.; Gu, Y.T.; Brown, R.J.; Senadeera, W. Numerical investigation of plant tissue porosity and its influence on cellular level shrinkage during drying. Biosystems Engineering 2015, 132 (0), 71-87.

26. Rathnayaka Mudiyanselage, C.M.; Karunasena, H.C.P.; Gu, Y.T.; Guan, L.; Senadeera, W. Novel trends in numerical modelling of plant food tissues and their morphological changes during drying – a review. Journal of Food Engineering 2017, 194, 24-39.

27. da Silva, W.P.; Rodrigues, A.F.; Silva, C.M.D.P.S.e.; Gomes, J.P. Numerical approach to describe continuous and intermittent drying including the tempering period: Kinetics and spatial distribution of moisture. Drying Technology 2017, 35 (3), 272-280.

28. Xu, Z.; Pillai, K.M. Modeling drying in thin porous media after coupling pore-level drying dynamics with external flow field. Drying Technology 2017, 35 (7), 785-801.

29. Xia, L.; Zhang, H.; Wang, B.; Yu, C.; Fan, X. Experimental and numerical analysis of oil shale drying in fluidized bed. Drying Technology 2017, 35 (7), 802-814.

30. Karunasena, H.C.P.; Senadeera, W.; Brown, R.J.; Gu, Y.T. A particle based model to simulate microscale morphological changes of plant tissues during drying. Soft Matter 2014, 10 (29), 5249-5268.

For Peer Review Only

31. Rahman, M.M.; Joardder, M.U.H.; Khan, M.I.H.; Nghia, D.P.; Karim, M.A. Multi-scale model of food drying: Current status and challenges. Critical Reviews in Food Science and Nutrition 2016.

32. Sobieski, W.; Dudda, W. Sensitivity analysis as a tool for estimating numerical modeling results. Drying Technology 2014, 32 (2), 145-155.

33. Aghbashlo, M.; Hosseinpour, S.; Mujumdar, A.S. Application of artificial neural networks (ANNs) in drying technology: A comprehensive review. Drying Technology 2015, 33 (12), 1397-1462.

34. Karunasena, H.C.P.; Senadeera, W.; Brown, R.J.; Gu, Y.T. Simulation of plant cell shrinkage during drying – a SPH-DEM approach. Engineering Analysis with Boundary Elements 2014, 44, 1-18.

35. Van Liedekerke, P.; Ghysels, P.; Tijskens, E.; Samaey, G.; Smeedts, B.; Roose, D., et al. A particle-based model to simulate the micromechanics of single-plant parenchyma cells and aggregates. Physical Biology 2010, 7 (2), 026006.

36. Van Liedekerke, P.; Ghysels, P.; Tijskens, E.; Samaey, G.; Roose, D.; Ramon, H. Mechanisms of soft cellular tissue bruising. A particle based simulation approach. Soft Matter 2011, 7 (7), 3580-3591.

37. Karunasena, H.; Hesami, P.; Senadeera, W.; Gu, Y.; Brown, R.J.; Oloyede, A. Scanning electron microscopic study of microstructure of gala apples during hot air drying. Drying Technology 2014, 32 (4), 455-468.

38. Mudiyanselage, C.M.R.; Karunasena, H.C.P.; Gu, Y.; Guan, L.; Banks, J., et al. A 3-D meshfree numerical model to analyze cellular scale shrinkage of different categories of fruits and vegetables during drying. In Proceedings of the 7th International Conference on Computational Methods, Berkeley, USA, August 1-4, 2016; 1070-1080.

39. O'Brien, T.P.; Feder, N.; McCully, M.E. Polychromatic staining of plant cell walls by toluidine blue O. Protoplasma 1964, 59 (2), 368-373.

40. Sakai, W.S. Simple method for differential staining of paraffin embedded plant material using toluidine blue o. Stain Technology 1973, 48 (5), 247-249.

41. Ray, S.F. Applied Photographic Optics: Lenses and Optical Systems for Photography, Film, Video, Electronic and Digital Imaging; Focal Press: 2002.

42. Brecko, J.; Mathys, A.; Dekoninck, W.; Leponce, M.; VandenSpiegel, D.; Semal, P. Focus stacking: Comparing commercial top-end set-ups with a semi-automatic low budget approach. A possible solution for mass digitization of type specimens. ZooKeys 2014, 464, 1.

43. Schneider, C.A.; Rasband, W.S.; Eliceiri, K.W. NIH Image to ImageJ: 25 years of image analysis. Nature Methods 2012, 9 (7), 671-675.

44. Abràmoff, M.D.; Magalhães, P.J.; Ram, S.J. Image processing with imagej. Biophotonics International 2004, 11 (7), 36-42.

45. Pante, M.C.; Muttart, M.V.; Keevil, T.L.; Blumenschine, R.J.; Njau, J.K.; Merritt, S.R. A new high-resolution 3-D quantitative method for identifying bone surface modifications with implications for the early stone age archaeological record. Journal of Human Evolution 2017, 102, 1-11.

46. Digital Surf. Mountains® surface imaging & metrology software 2017 [cited 2017 13 May]. Retrieved from: http://www.digitalsurf.fr/en/mntkey.html.

For Peer Review Only

47. Ho, A.; Jorns, B.; Mikellides, I.G.; Goebel, D.M.; Lopez Ortega, A. Wear test demonstration of a technique to mitigate keeper erosion in a high-current lab 6 hollow cathode. In Proceedings of 52nd AIAA/SAE/ASEE Joint Propulsion Conference, Salt Lake City, USA, July 25-27, 2016; 4836.

48. Asgharifar, M.; Mazar Atabaki, M.; Kovacevic, R. Characterization of the surface topography of arc-treated aluminum alloys by fractal geometry. Manufacturing Letters 2014, 2 (2), 26-29.

49. Doymaz, İ.; Kocayigit, F. Drying and rehydration behaviors of convection drying of green peas. Drying Technology 2011, 29 (11), 1273-1282.

50. Wang, C.; Wang, L.; Thomas, C. Modelling the mechanical properties of single suspension-cultured tomato cells. Annals of Botany 2004, 93 (4), 443-453.

51. Gao, Q.; Pitt, R. Mechanics of parenchyma tissue based on cell orientation and microstructure. Transactions of the ASAE 1991, 34(1), 232-238.

52. Pitt, R. Models for the rheology and statistical strength of uniformly stressed vegetative tissue. Transactions of the ASAE 1982, 25 (6), 1776-1784.

53. Wu, H.-I.; Spence, R.D.; Sharpe, P.J.H.; Goeschl, J.D. Cell wall elasticity: I. A critique of the bulk elastic modulus approach and an analysis using polymer elastic principles. Plant, Cell & Environment 1985, 8 (8), 563-570.

54. Karunasena, H.C.P.; Hesami, P.; Senadeera, W.; Gu, Y.T.; Brown, R.J.; Oloyede, A. Scanning electron microscopic study of microstructure of gala apples during hot air drying. Drying Technology 2014, 32 (4), 455-468.

55. Rahman, M.S. Toward prediction of porosity in foods during drying: A brief review. Drying Technology 2001, 19 (1), 1-13.

56. Rahman, M.S.; Dehydration and microstructure. In Advances in Food Dehydration; Ratti, C., Ed.; CRC Press: 2008; 97-122.

57. Karunasena, H.; Gu, Y.; Brown, R.; Senadeera, W. Numerical investigation of case hardening of plant tissue during drying and its influence on the cellular-level shrinkage. Drying Technology 2015, 33 (6), 713-734.

58. Wang, N.; Brennan, J. Changes in structure, density and porosity of potato during dehydration. Journal of Food Engineering 1995, 24 (1), 61-76.

59. Rahman, M.S.; Al-Zakwani, I.; Guizani, N. Pore formation in apple during air-drying as a function of temperature: Porosity and pore-size distribution. Journal of the Science of Food and Agriculture 2005, 85 (6), 979-989.

60. Ratti, C. Shrinkage during drying of foodstuffs. Journal of Food Engineering 1994, 23 (1), 91-105.

61. Bai, Y.; Rahman, M.S.; Perera, C.O.; Smith, B.; Melton, L.D. Structural changes in apple rings during convection air-drying with controlled temperature and humidity. Journal of Agricultural and Food Chemistry 2002, 50 (11), 3179-3185.

For Peer Review Only

Table 1: Variation of surface roughness (S_a), maximum height (S_z) and the root mean square height (S_q) with the normalised moisture content (X/X_0) for a selected apple sample at different states of dryness (Corresponding standard deviations (SD) included)

Time (min)	X/X_0	SD (%)	S_a (µm)	SD (%)	S_z (µm)	SD (%)	S_q (µm)	SD (%)
0	1.0000	0.0	31.7	14.6	164.0	16.8	37.3	16.8
3	0.8429	14.7	35.4	15.5	171.0	17.5	41.5	18.4
6	0.6339	17.3	29.4	14.3	147.0	16.4	35.2	17.2
9	0.4706	16.6	24.4	13.8	125.0	12.6	29.3	15.1
12	0.3622	16.8	24.0	14.7	150.0	13.9	30.1	14.2
15	0.2701	12.4	25.0	18.7	140.0	17.9	31.6	15.2
18	0.1819	11.9	25.8	16.9	134.0	15.1	32.2	14.6
21	0.1138	10.2	24.7	18.5	131.0	16.3	31.0	19.4
24	0.0611	18.0	24.4	19.6	150.0	17.5	31.5	21.0
27	0.0364	22.9	25.0	14.3	137.0	15.3	31.9	14.4
30	0.0186	16.6	22.2	25.2	107.0	22.4	27.1	19.2
33	0.0077	17.2	24.7	24.7	132.0	23.3	31.0	21.8
36	0.0046	12.2	24.9	18.1	131.0	22.1	31.1	19.3
39	0.0015	15.3	25.2	15.5	137.0	15.0	31.6	15.1
42	0.0000	0.0	25.2	17.4	130.0	16.8	31.3	17.0

For Peer Review Only

Table 2: The quantified morphological properties for a single cell along with the corresponding time and moisture content variations (Corresponding standard deviations (SD) included)

Time (min)	X/X_0	SD (%)	A/A_0	SD (%)	D/D_0	SD (%)	R/R_0	SD (%)
0	1.000	0.0	1.000	0.0	1.000	0.0	1.000	0.0
3	0.910	35.5	0.960	17.5	0.980	19.9	1.010	12.4
6	0.768	33.1	0.950	16.0	0.970	13.6	1.010	17.0
9	0.608	23.8	0.930	12.2	0.970	16.9	1.010	15.1
12	0.464	49.2	0.920	24.0	0.960	12.8	1.000	9.2
15	0.267	41.5	0.860	20.2	0.930	22.4	1.000	14.2
18	0.172	29.9	0.880	14.0	0.940	16.1	0.990	12.9
21	0.092	34.8	0.870	17.8	0.930	15.3	1.000	10.6
24	0.035	35.6	0.860	18.8	0.920	19.5	1.000	18.0
27	0.010	43.5	0.830	21.9	0.910	20.2	1.010	1.5
30	0.003	32.9	0.820	16.0	0.910	17.3	1.010	18.9
33	0.001	30.1	0.810	15.9	0.900	16.4	0.990	14.0

For Peer Review Only

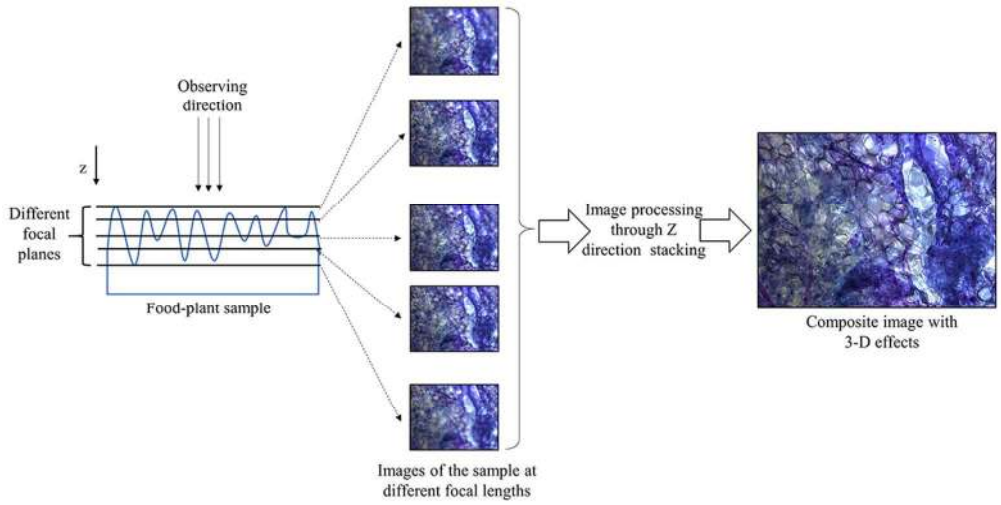

Fig. 1: The process to obtain a 3-D image through a series of images at different focal lengths (z-stacking or focus stacking) (Note: the real number of images taken for z-stacking is much larger than shown here)

101x51mm (300 x 300 DPI)

Review Only

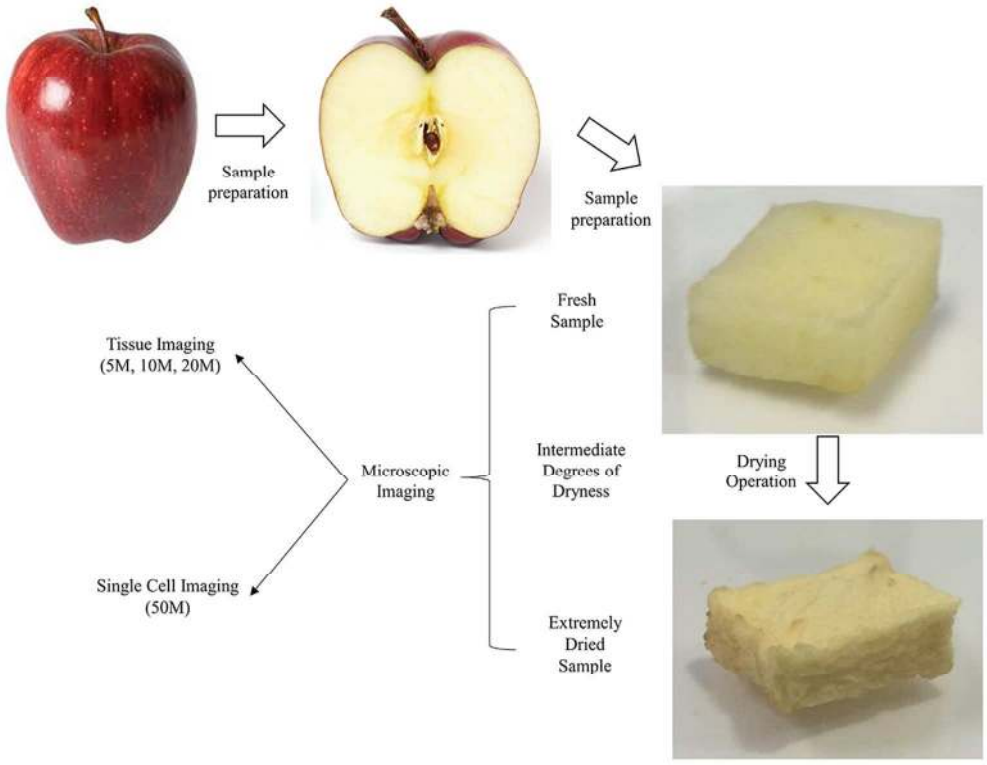

Fig. 2: Experimental procedure undertaken in this study: from the fresh fruit through the sample preparation and drying process to the microscopic imaging at different magnifications (i.e. 5M, 10M etc.)

101x80mm (300 x 300 DPI)

w Only

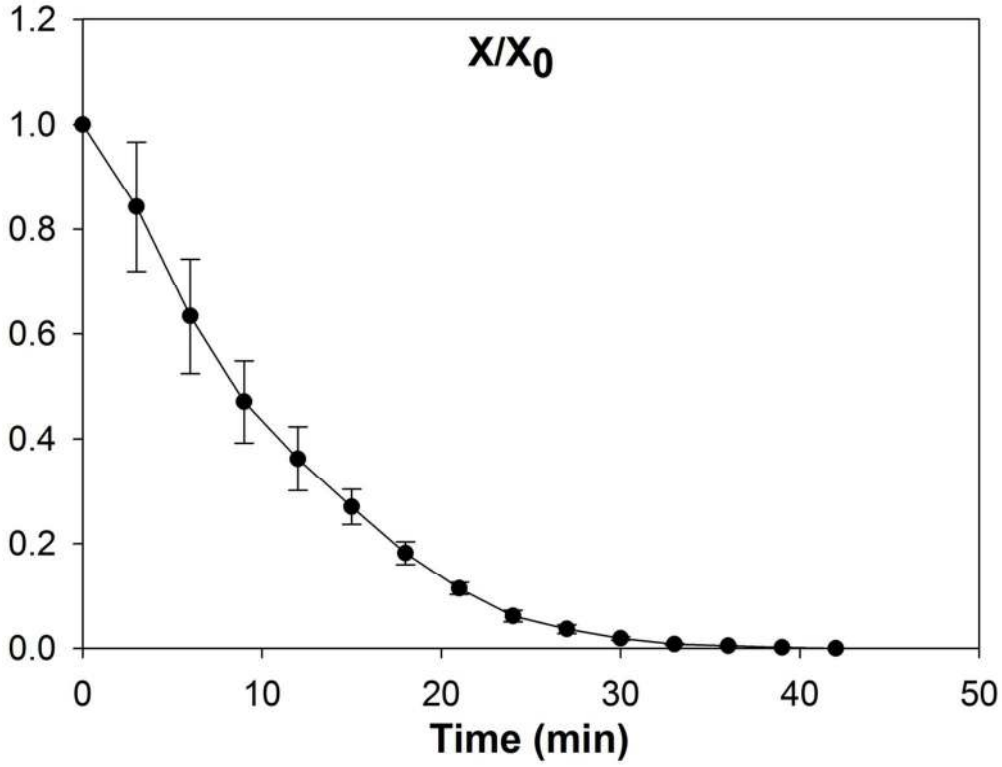

Fig. 3: The drying curve elaborating time variation of the normalised moisture content (X/X_0) during the whole drying cycle

108x83mm (300 x 300 DPI)

For Review Only

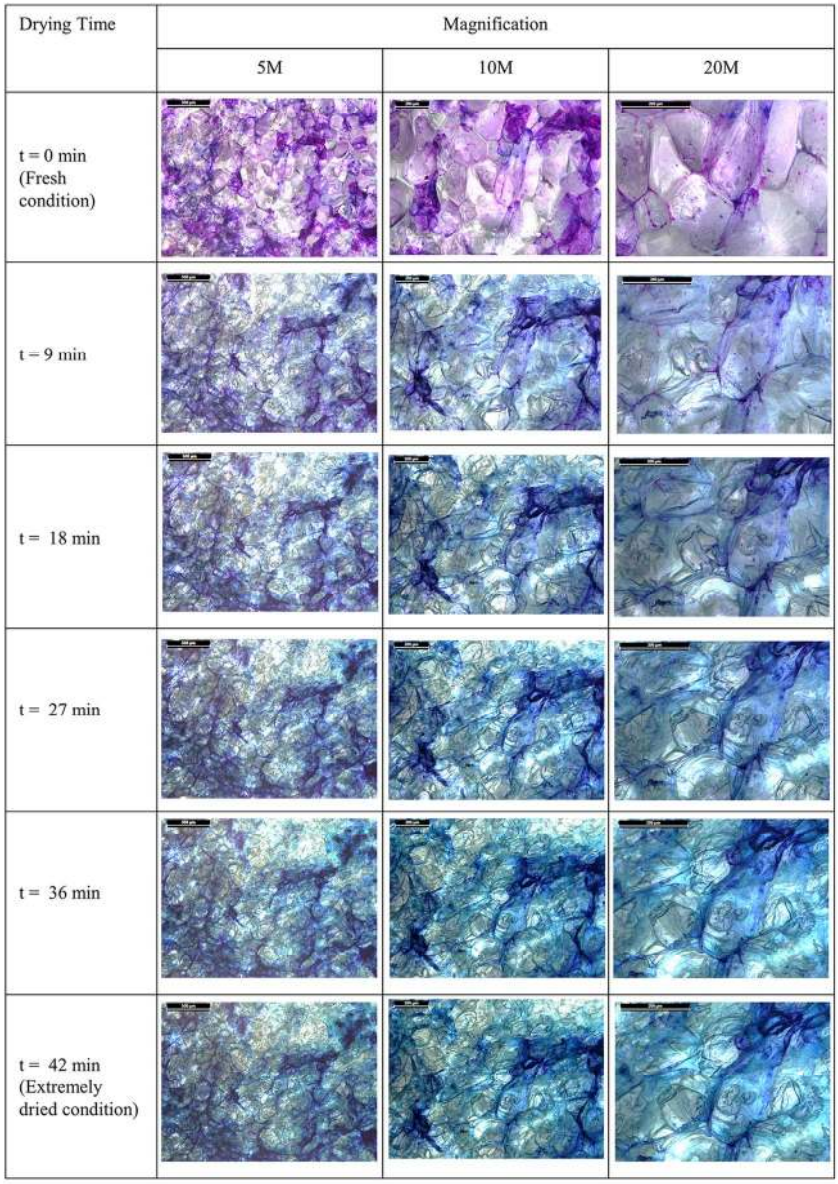

Fig. 4: Digital light microscopy images of apple tissues at different dryness states imaged using different magnifications

108x152mm (300 x 300 DPI)

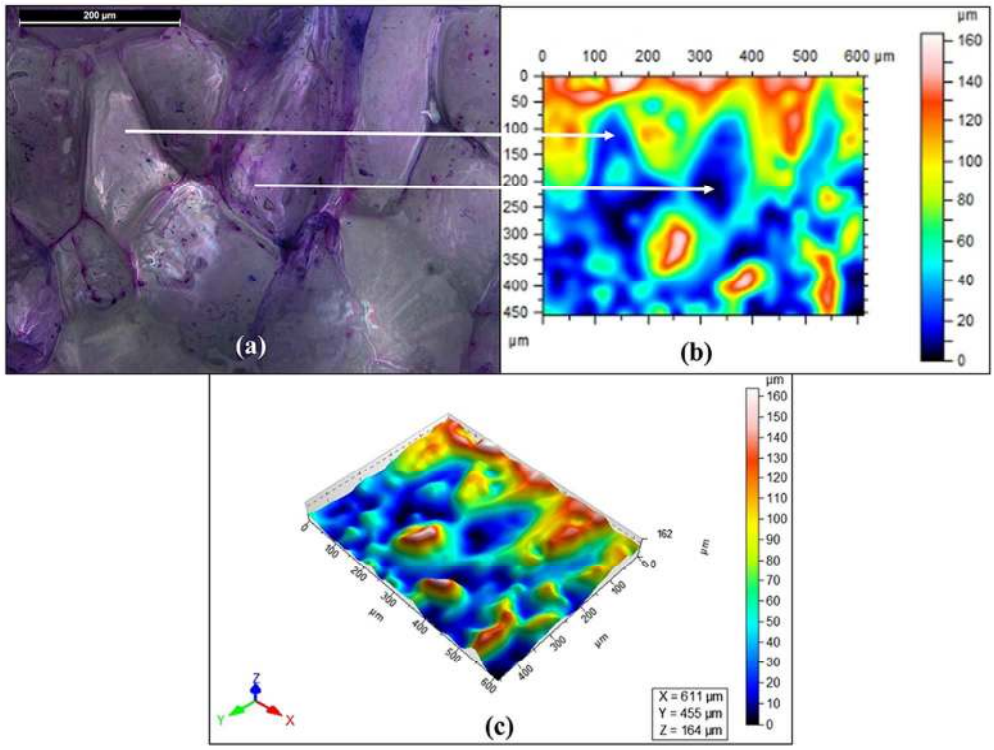

Fig. 5: 3D contour map corresponding to the 20M image taken for the fresh apple sample: (a) Microscopic image for fresh apple tissue at 20M; (b) 3-D contour map obtained through 'Nanovea Expert 3D' for the same sample; (c) The isometric view of the 3-D contour map

101x77mm (300 x 300 DPI)

w Only

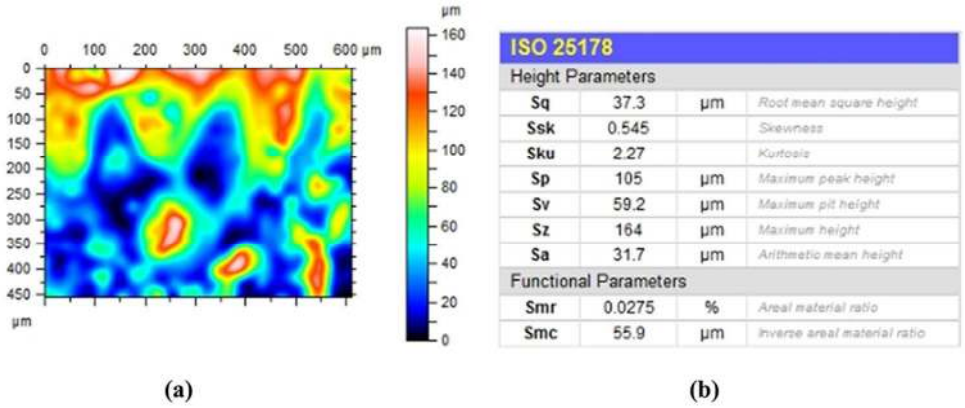

ISO 25178			
Height Parameters			
Sq	37.3	µm	Root mean square height
Ssk	0.545		Skewness
Sku	2.27		Kurtosis
Sp	105	µm	Maximum peak height
Sv	59.2	µm	Maximum pit height
Sz	164	µm	Maximum height
Sa	31.7	µm	Arithmetic mean height
Functional Parameters			
Smr	0.0275	%	Areal material ratio
Smc	55.9	µm	Inverse areal material ratio

Fig. 6: Surface information produced by Nanovea Expert 3-D software for a fresh apple surface: (a) Surface profile; (b) Surface parameter values

101x44mm (300 x 300 DPI)

For Review Only

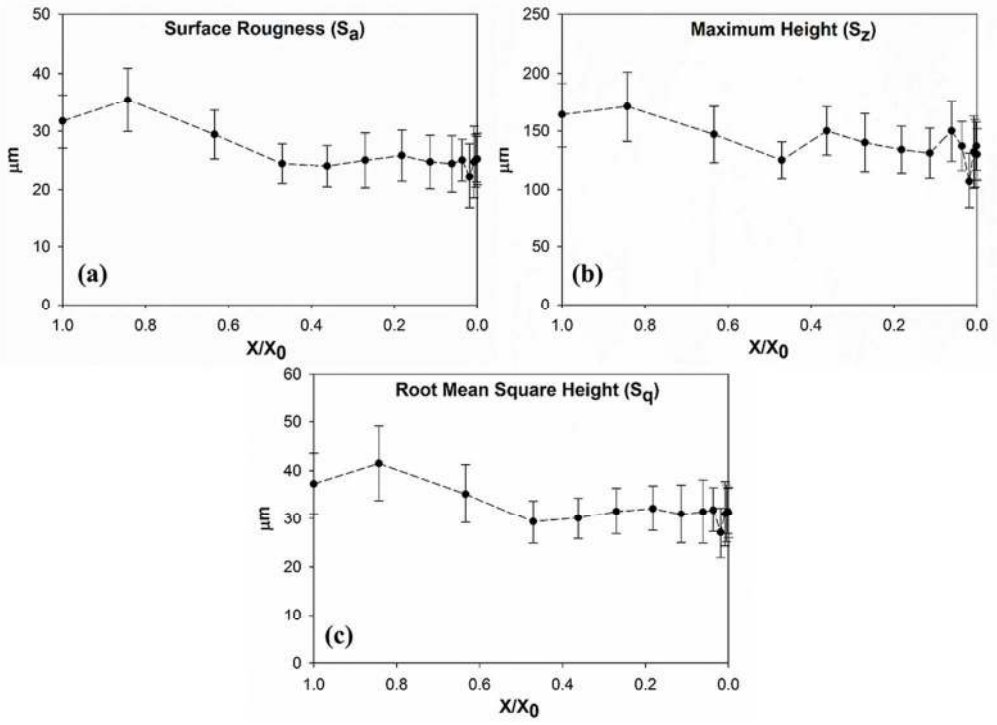

Fig. 7: Variation of: (a) Surface roughness (S_a); (b) Maximum height (S_z); and (c) Root mean square height (S_q) with the normalised moisture content (X/X_0) during drying

101x73mm (300 x 300 DPI)

For Review Only

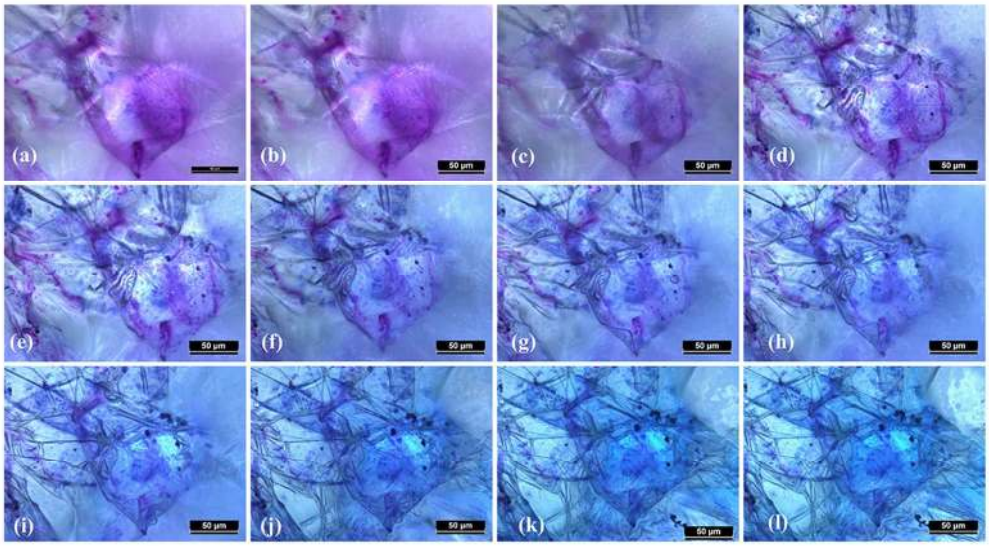

Fig. 8: Digital light microscopy images of a single cell: a (a) fresh cell; dried cell at (b) 3 min; (c) 6 min; (d) 9 min; (e) 12 min; (f) 15 min; (g) 18 min; (h) 21 min; (i) 24 min; (j) 27 min; (k) 30 min; (l) 33 min; min at a magnification of 50 (50M);

101x57mm (300 x 300 DPI)

For Review Only

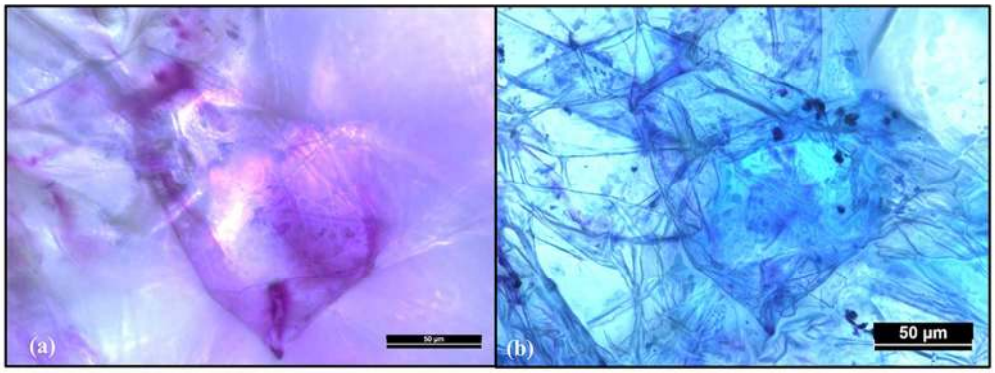

Fig. 9: Microscopic image of the single cell: (a) at fresh condition and (b) at extremely dried condition

101x38mm (300 x 300 DPI)

eer Review Only

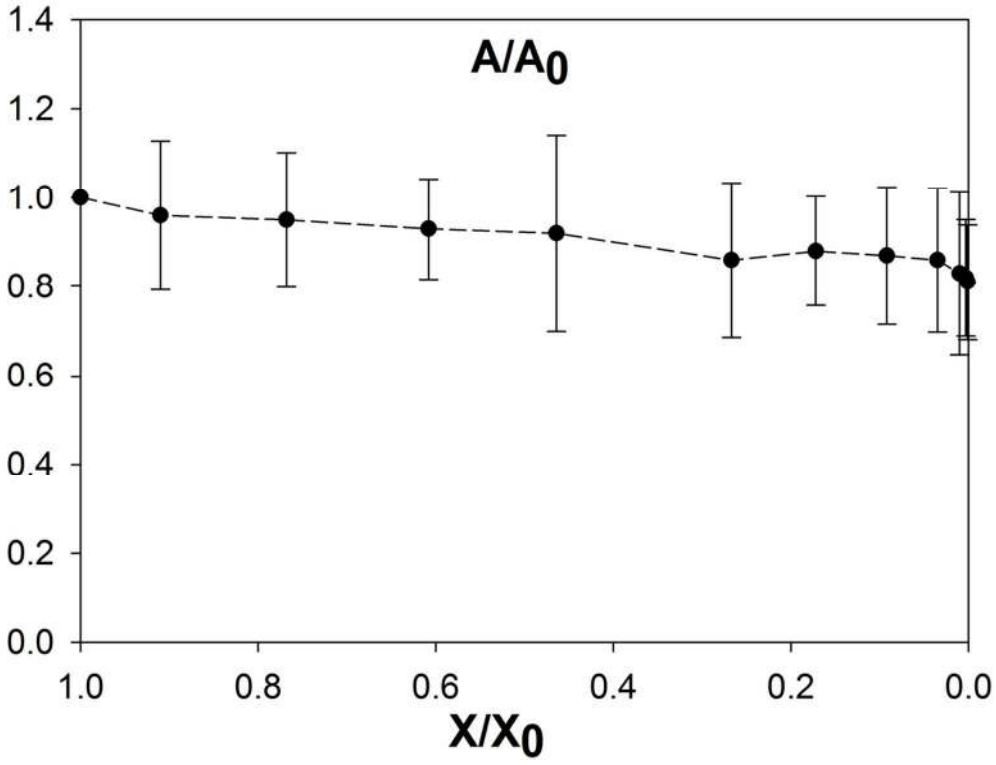

Fig. 10: Variation of the single cell area characteristics: normalised area (A/A_0) against normalised moisture content (X/X_0)

108x82mm (300 x 300 DPI)

For Review Only

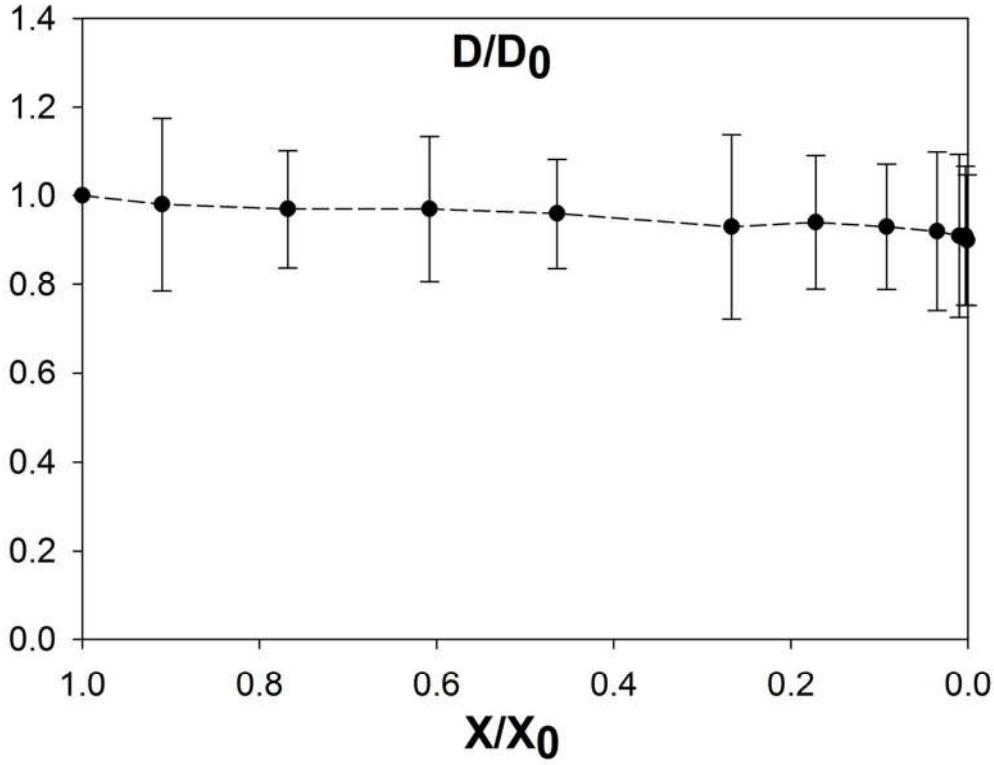

Fig. 11: Variation of the single cell area characteristics: normalised diameter (D/D_0) against normalised moisture content (X/X_0)

112x88mm (300 x 300 DPI)

w Only

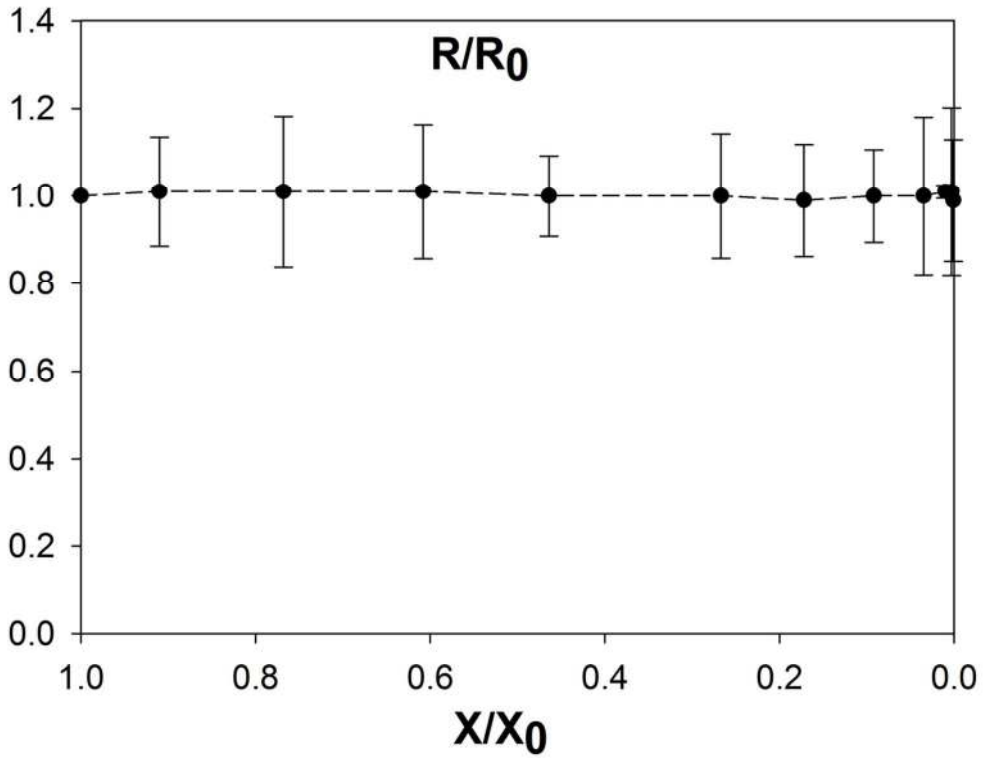

Fig. 12: Variation of the single cell area characteristics: normalised diameter (R/R_0) against normalised moisture content (X/X_0)

110x83mm (300 x 300 DPI)

For Review Only

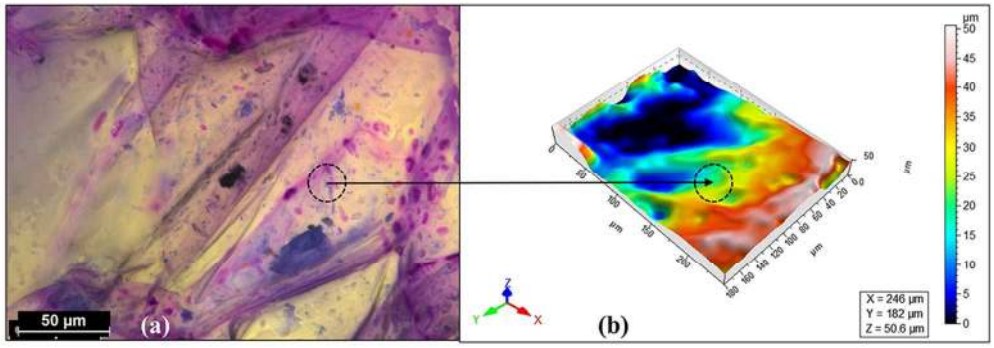

Fig. 13: 3-D contour map corresponding to the 50M image taken for the fresh apple sample: (a) Microscopic image for fresh apple cell (b) 3-D contour map obtained through 'Nanovea Expert 3D' for the same sample

101x36mm (300 x 300 DPI)

For Peer Review Only

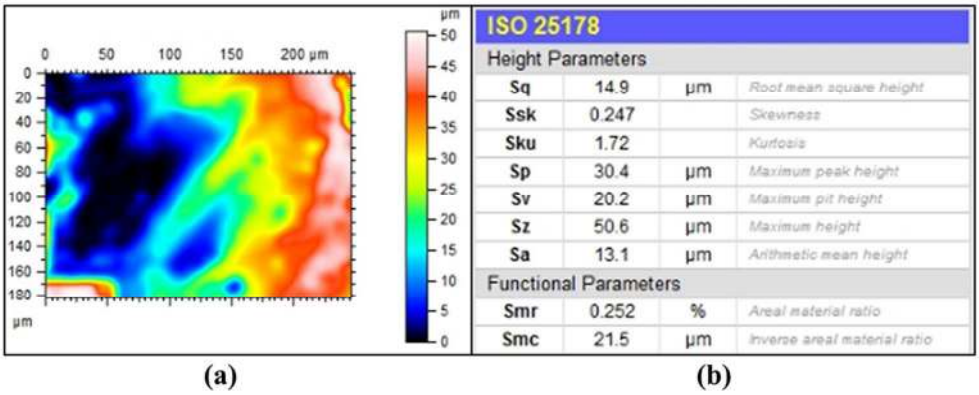

ISO 25178			
Height Parameters			
Sq	14.9	µm	Root mean square height
Ssk	0.247		Skewness
Sku	1.72		Kurtosis
Sp	30.4	µm	Maximum peak height
Sv	20.2	µm	Maximum pit height
Sz	50.6	µm	Maximum height
Sa	13.1	µm	Arithmetic mean height
Functional Parameters			
Smr	0.252	%	Areal material ratio
Smc	21.5	µm	Inverse areal material ratio

Fig. 14: 3-D surface texture analysis for the single cell microscopic image: (a) Surface profile; (b) Surface parameters

101x41mm (300 x 300 DPI)

er Review Only